The defect evolution in shock loaded tantalum single crystals

Pang, Bo; Case, S.; Jones, Ian; Millett, Jeremy C. F.; Whiteman, G.; Chiu, Yu-Lung; Bronkhorst, C. A.

DOI:
10.1016/j.actamat.2017.11.052

Accepted Manuscript

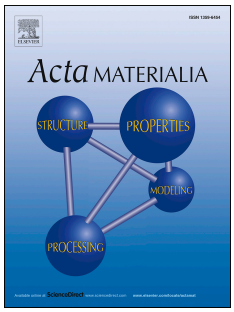

The defect evolution in shock loaded tantalum single crystals

B. Pang, S. Case, I.P. Jones, J.C.F. Millett, G. Whiteman, Y.L. Chiu, C.A. Bronkhorst

PII: S1359-6454(17)31043-1

DOI: 10.1016/j.actamat.2017.11.052

Reference: AM 14259

To appear in: *Acta Materialia*

Received Date: 24 July 2017

Revised Date: 29 August 2017

Accepted Date: 22 November 2017

Please cite this article as: B. Pang, S. Case, I.P. Jones, J.C.F. Millett, G. Whiteman, Y.L. Chiu, C.A. Bronkhorst, The defect evolution in shock loaded tantalum single crystals, *Acta Materialia* (2018), doi: 10.1016/j.actamat.2017.11.052.

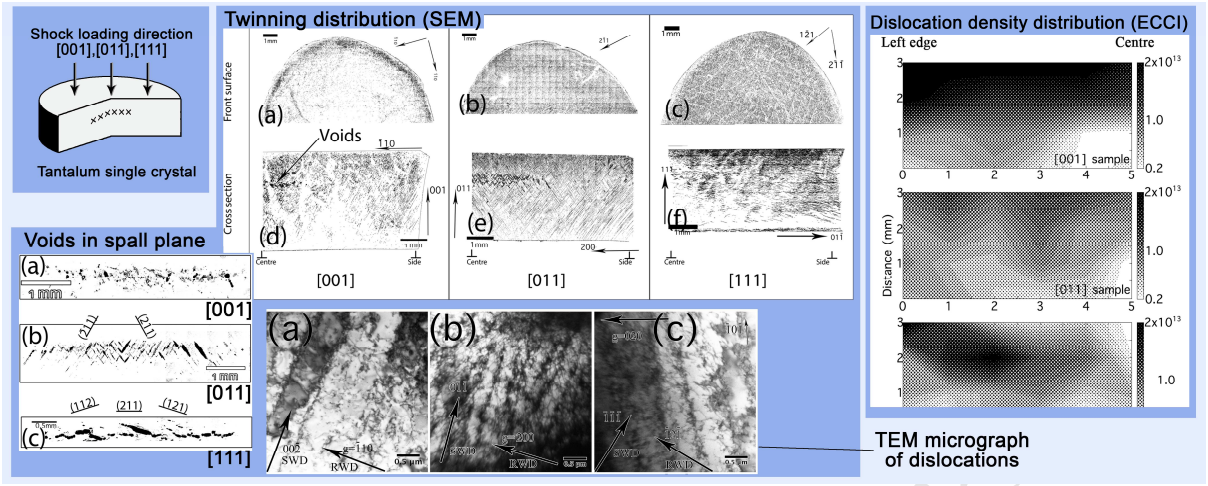

The defect evolution in shock loaded tantalum single crystals.

B. Pang[1], S. Case[2], I.P. Jones[1], J.C.F. Millett[2], G. Whiteman[2], Y.L. Chiu[1], C. A. Bronkhorst[3]

[1]School of Metallurgy and Materials, The University of Birmingham, Birmingham, United Kingdom

[2]AWE, Aldermaston, Reading, Berkshire, United Kingdom

[3]Theoretical Division, Los Alamos National Laboratory, Los Alamos, NM 87545, USA

Keywords: shock wave; plasticity; simulation; tantalum

Abstract

The defect structures of three different orientation ([001], [011] and [111]) shocked single crystals of tantalum have been characterised using scanning electron microscopy and transmission electron microscopy. The defect evolution and the response of the single crystals are found to be highly dependent on the orientation of the single crystals and the position in the specimen. Crystal plasticity simulation has been used to calculate the strain tensor in the specimens as a function of position and time. The defect types and distributions are analysed in terms of the shock wave and the lateral and back release waves. Twins at the sample centre and front surface were created by the shock wave front. The twins at the back of the sample close to the side surface are produced by the interaction of the release waves. Twinning area fraction and dislocation density are higher at the impact surface region than at the back surface due to decay of the elastic precursor and the difference in loading duration. Twinning

acts as a major deformation mechanism and has a strong influence on the Hugoniot elastic limit (HEL) and spall strength when the loading direction is [011] or [111].

1 Introduction

Tantalum (Ta) is a common refractory metal with a body-centred cubic crystalline structure and atomic number 73[1]. As a heavy metal with high strength and excellent ductility, tantalum is an ideal material to use in shaped charges and explosively forged projectiles (EFPs)[1][2]. These applications require a good knowledge of the deformation mechanisms of tantalum at high strain rate, including shock loading, especially the hardening behaviour and defect generation under high pressure shock compression and release.

Much research has been carried out on the deformation behaviour of tantalum under shock loading. The yield behaviour is strongly influenced by the microstructure and the shock conditions (e.g. grain size, deformation history and distance of travel of the shock wave). The Hugoniot elastic limit (HEL) of polycrystalline tantalum has been measured as 1-3 GPa[3][4][5]. Elastic precursor decay reduces the HEL with longer wave travel distance. At the shock interface, the HEL is the initial impact stress. The HEL decreases over the wave travelling distance and eventually falls down to the elastic limit of the material under quasi-static deformation conditions. The HEL of a material with a larger grain size decays faster than that for a smaller grain size[3]. Pre-shock deformation of a sample will decrease the HEL[3].

The work hardening of tantalum by shock is similar to the strengthening effect by quasi-static deformation to the same strain[6]. The dislocation substructures produced by shock in tantalum are similar to those after quasi-static deformation: screw dislocation dipoles, loops, heavily jogged dislocation tangles → dislocation cells[6][7][8][9]. The dislocation storage is rate-independent, only being related to the shock strain[6].

Twinning is frequently observed in tantalum after shock loading [10][11][12][8][13][14][6]. The tendency for twinning is high at high strain rate and low temperature, because the dislocation flow stress can effectively be raised up to the critical stress for twin formation. The threshold pressure for twinning in tantalum is still subject to debate as the experimental results are inconsistent. The measured threshold from laser compressed tantalum single crystals is 35GPa, below which pressure the stress required for dislocation slip is lower than the twinning nucleation stress[13]. Meyers calculated the theoretical critical pressure for twinning in tantalum using a constitutive model[15], giving a pressure in the range 35–71 GPa.

As a shear driven phenomenon, deformation twins can be strongly influenced by the shear stress during loading. It is reported that in 60 GPa shocked tantalum, twins were created preferentially in a region with higher wave obliquity (difference between wave travelling direction and stress), which means that the shock wave propagation direction is significantly different from the particle velocity and that the shear stress can be significantly increased[16]. There is however still a lack of knowledge of the effect of obliquity.

Most previous studies of the deformation behaviour of tantalum in shock loading were focused on the effect of the shock wave front on the residual

microstructure of the material. The release wave (either from the back surface of the projectile or the specimen) was considered to have a minor effect on the dislocation slip direction. This is because the loading direction of these release waves is the same as that of the shock wave and brings with it a lower strain rate. The lateral release wave has always been avoided in plate shock experiments and its significant effect on the plastic flow of material is not fully understood.

The hardening behaviour of polycrystalline tantalum under shock loading and quasi-static deformation has been extensively studied. However, the orientation dependence of the dislocation substructure evolution in single crystals under shock loading is still uncertain.

The objective of the work described in this paper was to understand the creation by shock of dislocations and twins in single crystals where lateral and longitudinal momentum trapping were not used and, therefore, shear stresses were more significant than usual. The resulting damage is not at all homogeneous and thus enables us, with the help of the modelling, to understand the importance of wave obliquity and the balance between dislocation slip and twinning in the response of the material.

2 Experimental procedure

The shock loading experiments were performed at AWE, UK. Tantalum single crystal (> 99.99%) discs with [111], [011] and [001] sample normal directions and a polycrystalline specimen were subjected to plate impact. The flyer plate was accelerated by a single stage gas gun to a velocity of 212 $m \cdot s^{-1}$. The thickness of the projectile was 3 mm. The samples had a diameter of 12 mm and a

thickness of 4 mm. Three single crystal discs with face normals [111], [011] and [001] were mounted in epoxy, together with a polycrystalline tantalum disc (50 mm diameter). Neither a momentum trap nor spall plates were used [17][18][6][19][20][21]. The velocity of the central area of the back surface of every disc was measured by a Heterodyne Velocimetry (HetV) system[22]. The three single crystals were recovered from the chamber for microscopic investigation.

The shocked single crystal discs were cut in half along the shock loading axis. The cutting plane for sample [001] was (110), for sample [011] was $(01\bar{1})$ and for sample [111] was $(2\bar{1}\bar{1})$. These planes were identified using electron backscattering diffraction (EBSD). The lateral surfaces of all the samples were ground using 'wet and dry' SiC paper from grit 400 to grit 4000. They were then subjected to polishing with OP-S polishing suspensions (Struers) for 1 hour. The polished surfaces were characterised using a Tescan Mira3 XM scanning electron microscope, working at 30kV beam voltage. The dislocation density distribution in the specimen was measured using the electron channelling contrast imaging (ECCI) technique which can provide images of dislocations in a SEM specimen across a large area. This technique is discussed in detail in another paper[23]. The distribution of the twins produced by the shock and release waves was characterised using backscattered electron imaging (BSE) and electron backscattered diffraction (EBSD). The BSE twin images were improved by FFT-ing, selecting the straight line perpendicular to the twin boundaries and then inverse FFT-ing.

TEM foils were cut from the centre and edge of the shocked discs parallel to the shock loading direction. The foils were thinned by electropolishing in an

electrolyte of 4% hydrofluoric acid, 20% sulphuric acid and 76% methanol at −25 ~ −30°C using a D.C. voltage of 25V. The focused ion beam technique is not employed here because the Ga^+ ions would not very effectively remove the Ta atoms due to their heavy mass, but instead create an amorphous layer at the surface of the foil. This makes the dislocation lines inside the foil difficult to distinguish, especially when the dislocation density is high.

TEM observations were carried out in a JEOL 2100 operating at 200kV. The Burgers vector analysis and trace analysis were performed according to the description by Loretto and Smallman[24]. The dislocations were imaged by TEM bright field imaging using two beam conditions.

3 Results

3.1 Wave propagation

The free surface velocity profile measured at the centre of the back surface of the specimens by the HetV is shown as a function of time in Figure 1. Using the equation of state (EOS) of the material under shock loading [25] and the EOS data for tantalum (C_0=3.293 km/s^{-1}, S_1=1.307)[26], the HELs of the [001], [011] and [111] samples are calculated to be 3.4 GPa, 2.2 GPa and 3.1 GPa.

After yielding, the free surface velocities show a significant drop and then a rise to 212 m·s^{-1} (6 GPa) at time 111.5 μs. This pressure holds for about 0.5 μs and then the velocity of the single crystals starts to drop to around 50 m·s^{-1}. The velocity of the back surface of the polycrystalline specimen holds for around 1.8 μs before it starts to drop. The velocities then oscillate between 50 m·s^{-1} and 170 m·s^{-1} for the next few microseconds. The single crystals with the same thickness as the polycrystalline sample have much shorter loading duration when

compared with the polycrystalline specimen. This is because the diameter of the single crystals is much smaller than that of the polycrystalline specimens: the lateral release wave can arrive at the centre of the back surface from the edge much more quickly than in the polycrystalline specimen. Therefore, the HetV curve of the single crystals shows much shorter wave duration. The polycrystalline Ta profile is not influenced by a lateral release wave. Detailed analysis and modelling of the free surface velocity profiles will be reported elsewhere [Whiteman, Case – to be published]. Further discussion here will concentrate on the resulting microstructures.

3.2 Spallation and Voids

The shock wave introduced profuse voids to the single crystal specimens. The voids appear as clusters located at the centre of every sample, around 1 mm away from the shocked interface. Stitched micrographs of the void clusters are shown in Figure 2.

The voids are mostly spherical in shape in sample [001], as shown in Figure 2(d). The voids in the samples [011] and [111] (shown in Figure 2(e)(f)) have coalesced and have an elongated elliptical shape. It should be noted that in samples [011] and [111], almost all the small voids are connected to twins. An example of this (in sample [011]) is shown at higher magnification (Figure 2(g)).

3.3 Twinning

The filtered twin micrographs were stitched together to show the distribution of twins across the sample. Figure 3(a) shows all the twins in the front surface of the [001] specimen. Only half of the sample is shown in the image because the distribution of the twins is symmetrical about the horizontal diameter. The twins

are very dense within 1 mm of the edge of the specimen. The density gradually decreases from the edge to the centre of the sample. The twins in the front surfaces of the [011] and [111] samples are however homogeneously distributed, as shown in Figure 3(b) and (c). The stitched image of the [001] sample cross-section with a beam direction $[\bar{1}\bar{1}0]$ is shown in Figure 3(d). It is found that the distribution of twins is strongly related to location in the specimen as summarised in Table 1, where every sample can be divided into three zones, shown in Figure 4: (1) front surface; (2) sample centre: front; (3) bottom region close to the outside surface.

3.4 Dislocations

The sampling regions for TEM observation are also shown in Figure 4. After electropolishing, the positions characterised by TEM are 1~1.5 mm below the front (shock) surface. For disc A the transparent region is 1-1.5 mm in from the side of the specimen, for disc B 1-1.5 mm from the centre of the specimen. The shock wave direction (SWD) and the release wave direction (RWD: the radial direction towards the centre of the sample) are defined in Table 2. The location of the sample area is represented by symbols A or B.

TEM micrographs from the shock loaded tantalum single crystals are shown in Figure 5. The dislocations in area B are generally heavily tangled. In the less tangled B areas, most dislocations are of near screw type. The dislocations in area A (close to the edge) form into dislocation walls (elongated dislocation cells) which are parallel to the shock loading direction in the [001] and [011] samples and are parallel to the [101] or $[\bar{1}2\bar{1}]$ directions in the [111] specimen.

The Burgers vectors of the dislocations in the tantalum TEM samples were studied using the g·b=0 extinction criterion. The results of the Burgers vector analysis are shown in Table 2. It should be noted that the dislocation Burgers vectors listed all have a major presence in the TEM observations; the rare dislocation Burgers vectors or those which cannot be distinguished from the dislocation wall contrast have not been listed. When using different g vectors, the dislocation densities appear to show no significant change, meaning that the Burgers vectors listed in the table are equally activated in the same specimen.

The longitudinal cross-section specimens through the tantalum single crystals were imaged using ECCI. As shown in Figure 6, the dislocation density is around 10^{13} m^{-2} close to the impact interface. It decreases with distance away from the shock interface, becoming $\sim 0.5\times10^{13}$ m^{-2} at the back surface. The dislocation density is generally higher at the sample edge than in the centre, especially at the front surfaces. The numbers of the dislocation densities should be regarded as relative only. The true numbers as measured by TEM are about ten times greater[27]. This is because ECCI has lower resolution than TEM and dislocation tangles can image as one dislocation. Also, dislocations coming straight out of the surface, which appear as a bright dot with a dark shadow, are not taken into account for dislocation density due to possible confusion with surface features. Therefore the dislocation density measured using ECCI inside one specimen is relative only, and much less than the true value.

3.5 Crystal plasticity simulation

Crystal plasticity simulation was used to calculate the resolved shear stress on the crystal planes in order to study the onset of the twins. 3-D simulations of a

tantalum plate, of thickness 3 mm, impacted at 212 m/s onto a single crystal tantalum target of thickness 4 mm were performed using the AWE Lagrangian hydrocode Pegasus[28]. A plate radius of 12 mm was used for both the impacter and target. Approximately 6 million cells were used, giving a cell length of 50 μm and a high spatial resolution. Simulations were run for a time of 30 μs (i.e. long after the initial shock has traversed the sample) in order to capture release and shock wave reverberations which may in principle induce twinning out to a late time.

The crystal plasticity model used here is that due to Anand and Bronkhorst[29], but with extensions to account for pressure dependence of the elastic moduli and dislocation drag processes. Similarly to other crystal plasticity shock studies[30], the pressure – elastic volume response is calculated using an equation of state, while deviatoric stresses are calculated via the crystal plasticity model. The model permits plastic slip on slip systems of the families {110} <111> and {112} <111>; 12 systems exist in each family, giving a total of 24 allowed slip systems. It is noted that twinning is not modelled here. The {112} <111> shear stress on relevant twinning planes is taken from the simulated shear stress for the identical slip plane. In this study, the modelled stresses (which take no account of twinning) are treated as an approximation in order to investigate the initiation of the twinning by the impact.

For ease of understanding, the highest shear stress experienced on the (211) $[\bar{1}11]$ system in sample [011] is shown in Figure 7(a), as a representative example of the twin systems activated in region (2) of the three single crystals (Figure 4). The time at which the maximum shear stress occurs is shown in Figure 7(b). This highest shear stress is when the shock wave front passes (at

time $\sim 0\ \mu s$). The amplitude gradually decreases with the depth of travel of the shock wave front. This is because, in the modelling, shear stress is largest where the plastic strain rate is largest, i.e. coincident with the shock wave front. As the shock wave propagates through the material, its risetime increases, and thus the associated strain rate decreases. This wave spreading is commonly seen in BCC materials e.g.[31]. Therefore the maximum shear stress encountered decreases from the impact interface to the back surface. For twinning systems activated in region (2) of the three single crystals, the simulation shows that the maximum shear stress is at the shock wave front.

Two more stress contour maps generated from the simulation are shown in Figure 8, as an example of twinning activated in region (3) of the three single crystals. A positive stress means a stress in favour of twinning and vice versa. Figure 8(a) shows the shear stress on the system $(\bar{2}11)$ [111] in the specimen [001] at time 0.69 μs. The shock wave front is around 1 mm from the sample back surface at this moment (see supplementary document for detailed x-t diagram). This agrees with the simulated map, where the yellow area indicates that the material compressed by the shock wave front is 1 mm from the back surface. The twinning systems (experimentally) activated in the bottom region close to the right outside surface (Figure 4 region (3)) were $(\bar{2}11)$[111] for sample [001]; $(\bar{2}11)$ [111] for sample [011] and (121) $[1\bar{1}1]$ for sample [111] (see Table 1). In the contour map Figure 8(a), the right side of the sample has a negative stress (i.e. shear stress in anti-twinning direction). Similar negative stresses were found in the simulation of $(\bar{2}11)$ [111] for sample [011] and (112) $[11\bar{1}]$ for sample [111]. This means that when the shock wave enters the material, the stresses in the region (3) of the samples do not favour the

nucleation of the twins which are eventually produced in this region. Conversely the interaction of the back/side release waves creating the highly positively stressed region for these twinning systems appears on the right side. This could well be when the twins in region (3) started to nucleate and grow. This phenomenon is shown in Figure 8(b). After the interactions of the release waves, the overall amplitude of the waves gradually decreases, becoming much lower than at the shock wave front.

4 Discussion

4.1 Spallation and voids

In the HetV free surface profile (Figure 1), the material is not fully decelerated to zero velocity after unloading by the release waves. This suggests that spallation takes place[25][32][33]. The void clusters in the three single crystals are all around 1 mm beneath the impact interface, which is where the two release waves from the back surfaces of projectile and specimen interact for the first time (at t = 2.1μs). The void clusters are generated by the tensile stress formed by the two back release waves.

The [001] direction is stronger with respect to the tension created by the release wave interaction. This is mainly because in the [001] sample fewer voids are generated by spall. The release suffers a minor energy loss in creating the surface energy of the voids, i.e. the plastic deformation accomplishing the void growth in the [001] sample is smaller than in the other two because the total dimension of the cluster in the [001] sample is much smaller than in [011] or [111] for reasons which will be discussed later.

The creation of a ductile fracture in shock loaded ductile material often consists of three stages: (1) voids nucleate at second phase particles/ grain boundaries/ twin boundaries, followed by (2) void growth and (3) void coalescence[34][35][36][37]. From Figure 2 it can be seen that sample [001] is still in phase (2) since coalescence is not yet observed. The voids in the [011] and [111] samples show an elongated morphology, with the long axis parallel to the twins. This indicates that samples [111] and [011] are in phase (3): void coalescence.

Figures 2(e) and (f) show SEM BSE images of typical void morphologies in [111] and [011] samples. Figure 2(f) shows a lot of small voids on deformation twins in the [111] sample. It is found that almost all the small voids are connected to twins, suggesting that the onset of these voids is at the twin boundaries. Figure 2(e) shows a cluster of connected voids lying in the $[\bar{2}11]$ direction. A very long twin penetrates the whole cluster along the long axis. The centres of some voids are connected to a (211) twin, as shown in Figure 2(g). The voids are possibly nucleated at the junctions of the (211) and $(\bar{2}11)$ twins and grow and link together to form an elongated cluster as shown in Figure 2(e). This suggests that the twins in the [011] and [111] samples appear before ductile fracture, i.e. the twinning is created by the shock wave front in the [011] and [111] specimens. This phenomenon is also observed by Livescu et al., who found voids generated at twin boundaries in explosively driven shocked tantalum[14]. Previous modelling work (Wang[38], Hahn et al. [39][40]) shows that voids can be nucleated from twin boundaries by stress concentration when twins interact with other twins or dislocations. The relationship between the voids and the twins will be discussed further in the next section.

4.2 Twinning

The relationship between twinning planes and stress

Region (2): In section 4.1 above it was suggested that the twins in region (2) (Figure 4) of the [011] and [111] samples are created by the shock wave front. Crystal plasticity simulation (Figure 7(b)) shows that the highest resolved shear stress for the twinning system that activated in region (2) is at the initial shock wave front. The twinning planes of the systems with the highest shear stress in the [001] sample are $(2\bar{1}1)$, (211), (121), $(\bar{1}21)$, $(2\bar{1}\bar{1})$, $(21\bar{1})$, $(12\bar{1})$ and $(\bar{1}2\bar{1})$. For [011] they are (211) and $(\bar{2}11)$. For the [111] sample they are (112), (121) and (211). The twins in region (2) of the three single crystal samples are on *exactly these planes*, as shown in Table 1. This confirms that it is the high resolved shear stress at the shock front that produces the twins in region (2) of all the specimens.

Region (3): Region (3) in Figure 4 has a different twin distribution from region (2) in all the three single crystal specimens. This region experiences high shear stresses created by the lateral release wave. Figure 8(a) shows the simulated shear stress on plane $(2\bar{1}\bar{1})$ when the shock wave front passes through sample [001]. The stress does not favour twinning in region (3) (although it is not zero). Figure 8(b) shows the stress map from just after the interaction of the first set of back release waves. The high resolved shear stress regions generally overlap with the twinning in region (3) of sample [001]. Thus the twins in region (3) may be created by the interaction of the first set of release waves. This finding is similar for samples [011] and [111].

Region (1): For the [011] and [111] samples, region 1 (Figure 4) behaves in the same way as region 2. The twins are evenly distributed across the impact interface, except for some edges with strong plastic flow during the shock impact so that the twins cannot be distinguished clearly in the SEM micrographs. In region 1 (front surface) of the [001] sample, twins were rarely found in the centre of the specimen. Instead they form a ring at the edge of the specimen which indicates that the nucleation and growth of the twins in this area are strongly affected by the lateral release wave. We do not fully understand the reason for this phenomenon.

Area fraction of twinning

Beside the difference in twin types between areas (2) and (3), another significant feature of the twinning distribution is that the twin area fraction decreases with distance from the sample front surface. Over the time period of the shock wave compression, the material in area (2) of all the specimens experienced the same compression pressure of 6.13 GPa. Therefore, there are only two reasons that can possibly cause the differences in twinning area fraction: (1) a variation in the shock loading duration; (2) the elastic precursor decay.

The effect of shock pulse duration on deformation twinning was first explored by Appleton and Waddington[41]. Murr[42] suggested that the primary effect of longer pulse duration in shock is mainly allowing the dislocations to have time for movement, interaction and equilibration, thereby increasing the amount of dislocation-assisted twinning nucleation and growth as originally proposed by Cohen and Weertman[43].

The elastic precursor decay is a phenomenon whereby when a shock wave travels through a material, the Hugoniot elastic limit (HEL) will decrease with the travel distance of the shock wave front due to the high density of mobile dislocations produced by the shock wave front[44].

The calculation of the elastic precursor decay in tantalum was developed by Gillis[45], following developments in the dynamic yielding theory and dislocation dynamics [46][47]. The calculated HEL decays are shown in Figure 9. It should be noted that Gillis's model for the elastic precursor decay does not consider twinning or non-Schmid stress effects[48]. This could change the characteristic drag stress of the material (D^*) (More detailed modelling of HEL magnitude and precursor decay will be presented in a future article [G. Whiteman and S. Case, to be published]). Therefore a factor was added to D^* to adjust the value of the HELs to fit the experimental measurements. The revised D^* can be written as: $D_r^* = kD^*$, where k is a correction factor related to the effect of twinning and/or non-Schmid stress effects on the HEL. The drag factors for the [001], [011] and [111] samples are now 1.32, 0.67 and 0.85, respectively. The profile of the area fraction of the twinning in the area (2) of every sample is also plotted in the same figure 5, against distance. The bottom figure shows the shock loading duration as a function of distance. It should be noted that in the twin area fraction plot, there is no data in the range 0.5 mm to 1.5 mm because the image contrast is strongly influenced by the voids: the twins cannot be identified.

The twin area fraction in the [011] sample is generally higher than in the other two. This was also found in the molecular dynamic study performed by Ravelo et al.[49] and in experimental work by Florando and Barton[12], which show that twinning is more pronounced in shock along the <011> direction than

the <001> and <111> directions: no convincing explanation for this is offered. However, the Schmid factor for twins in the [011] sample is much higher than those for the [001] and [111] directions (Table 3): this could be the reason why twinning in [011] sample is a more pronounced deformation mechanism than for the other two loading directions. The twinning area fraction decreases rapidly from the shock impact interface over the front 0.5 mm in the [011] and [111] samples. This is probably due to the strong decay of the elastic precursor in this area. As the HEL decreases, the flow stress of the dislocations is reduced and the material slips more easily, therefore less strain is accommodated by twins. Therefore fewer twins are produced in the region with lower HEL. In the range from 1.5 mm to 4 mm, even though the reduction in the HEL is small, the twinning area fraction in the [011] sample still decreases quickly. The loading duration plot (Figure 9) shows that the duration of the shock loading between 1.5-4 mm decreases quickly from 1.7 μs to 0. This suggests that the decrease in the area fraction of twins in this region is due to the reduction in the shock wave loading duration.

The twinning in the [001] sample shows a very different distribution from the other two orientations. The area fraction at the shock interface is close to zero. It slowly increases to around 2.5% at 0.5 mm and then decreases with distance. The very low density of twinning in the shock impact interface suggests that the shock front does not find it easy to create twins in the [001] sample. The peak of the twinning area fraction at 0.5 mm shows that there is a concentration of twin nucleation/growth at this depth. However, over the time period of the first compression loading cycle, there is no difference in loading between x = 0 mm and x = 0.5 mm, except via the reduction of the HEL. One possibility is that the

twinning is created at the shock front, but because there are too many twinning systems activated at the same time (8 different planes), they cannot grow too much in length over the first compression cycle (before the void nucleation). Therefore the void clusters cannot grow in a specific orientation (as they do in [011] and [111]). This can also explain why the spall strength of the [001] sample is stronger than for the other two specimens, because the voids have fewer sites (twin boundaries) to nucleate on and fewer voids lead to a higher spall strength. Another possibility is that there was machining damage at the front surface of the [001] sample: this would increase the local dislocation density and reduce the likelihood of twinning since more mobile dislocations are available. [011] sample has a similar, but smaller, trend at the front surface (see Figure 9).

4.3 Dislocations

Dislocation morphology

The dislocation morphology in the three single crystals depends markedly on position (Figure 5). Close to the centre (region B), the dislocations are loosely tangled and consist of long straight screw dislocations with curly dislocation loops/debris in between. A TEM study of 7–20 GPa loaded polycrystalline tantalum reported by Gray and Vecchio[6] shows a very similar dislocation substructure. The loose dislocation tangles in region B (see Figure 4) of the three single crystals in the current study have the same characteristics as the tantalum shocked by Gray and Vecchio to 20 GPa. The density of the tangles and the dislocations in the current study are higher than in Gray's 7 GPa shocked sample. Because Gray's specimen was protected by momentum rings/disks, it was free

from the influence of the release waves. Therefore the higher dislocation/tangle density in region B of the 6.13 GPa shocked single crystals of this research is likely to have been induced by the lateral/back release waves.

It is notable from Figure 5 that the dislocation walls form only in the outer part of the specimen. Also, they do not depend on the orientation of the crystal: they are parallel (in the case of [001] and [011]) or nearly parallel (for [111]) to the shock direction and perpendicular to the radial direction. They are not present in the middle of the specimen, so cannot be caused by the principal shock wave. They are presumably caused by the radial release wave. This returns many times and the process of forming the walls may be akin to that in fatigue where dislocation walls also are formed.

Slip systems

Comparing with the results from TEM Burgers vector analysis in Table 2, it is found that except for region B of the [011] sample, the Burgers vectors are all different from the Schmid factor predictions. Thus, the slip in the material must be influenced by a combination of the back release wave and the lateral release wave.

Dislocation density

Although the dislocation substructure is changed by the release waves, the dislocation density measured using ECCI still decreases from the sample front surface to the back surface. Usually, in plastic deformation, the material experiencing more plastic strain/stress will have a higher dislocation density, because the plastic strain is accomplished by dislocation multiplication and movement[50]. If the dislocation velocity is the same (under the same

pressure/stress), the plastic strain of the material depends on dislocation multiplication. The area close to the shock front surface spends longer in a high pressure compressed or tensioned state, compared to the rear of the sample. The pressure in the region close to the back surface is usually lower because it is close to a free surface where no stress is applied. Also, similar to the hypothesis for the twinning distribution, shock wave precursor decay can lead to variations in residual dislocation density. As the shock wave moves, the plastic wave spreads out and the strain rate of the shock wave front is lower at the back surface than at the impact surface. The reason for the front-back dislocation density distribution can be summarised to be: (i) loading duration; (ii) shock wave precursor decay and (iii) strain rate difference caused by wave partitioning.

The dislocation density rises at the edge of the sample front surface (Figure 6) are due to the lateral plastic strain caused by the lateral release wave. When the shock wave is just entering the material at time 0.2μs, the lateral surfaces of the specimen and the projectile are perfectly parallel. As the lateral release waves move into the sample, the material of both sample and projectile close to the shock interface starts to deform outwards. The material at the back surface is also loaded by the lateral release wave, but does not see a lot of lateral strain. This is because the shock wave reflects from the sample back surface and transfers to a back release wave, which interacts with the lateral one and reduces the radial velocity and the tensile stress in the lateral direction. This makes the material at the back surface move mainly along the shock wave direction and therefore experience a lower lateral strain than the front surface. This strain can be seen in the filtered twinning images in Figure 3(d) and (f) where the upper

right corner has deformed outwards by around 0.2 mm. This extra strain is the reason why the dislocation density is particularly high at the edge of the shock loading interface.

5 Conclusions

The plate impact shock experiment used here generated a 6.1 GPa shock wave front. The material experienced loading from the shock wave, a lateral release wave, a back release wave and their interactions/reflections. The shock wave front created profuse deformation twinning in the three single crystals.

In the [011] and [111] samples, twinning acts as a major deformation mechanism at the shock wave front. In the [001] sample, twinning is nucleated at the shock wave front but has lower area fraction than [011] and [111] samples, possibly due to the influence of the twin-twin interaction and smaller Schmid factor. The deformation twinning (or non-Schmid stress) may have influenced the HEL of the material. The HetV measured HELs for the [001], [011] and [111] samples were 3.17 GPa, 2.23 GPa and 3.08 GPa. The calculated dislocation flow drag factor shows that the effect of deformation twinning on the [001] sample is hardening, but softening on the other two. The twinning produced in region (2) of all three samples followed Schmid's law. However, in region (3) the nature of the twins is rather complex under the combination of back and lateral release waves. Crystal plasticity simulation indicates that the twins in region (3) are probably created by the interaction of the first set of release waves.

The interaction of the back release waves created voids in the tantalum single crystals. The voids in sample [111] and [011] nucleated and grew along the twinning boundaries. In the [001] sample, fewer voids were created due to lack

of pre-existing nucleation sites (twins) created by the shock wave front, probably because the small RSS and interaction of 8 twinning systems suppresses the growth of twins. The lack of voids gave the [001] sample a higher spall strength than the [011] and [111] specimens.

ECCI dislocation density measurements show that more dislocations are created in the region close to the shock interface and confirmed that the lateral release wave induced extra lateral strain. The dislocation structure, density and slip systems are heavily influenced by wave reflection and interaction.

We have been able to exploit here the absence of momentum trapping to understand better twin formation in shocked tantalum, its spatial distribution and when it occurred. To understand dislocation formation to the same degree, however, will require single crystals with effective momentum trapping in both the shock/lateral directions.

6 Acknowledgement

7 References

[1] S.M. Cardonne, P. Kumar, C.A. Michaluk, H.D. Schwartz, Tantalum and its alloys, Int. J. Refract. Met. Hard Mater. 13 (1995) 187–194.

[2] V.F. Nesterenko, M.A. Meyers, J.C. LaSalvia, M.P. Bondar, Y.J. Chen, Y.L. Lukyanov, Shear localization and recrystallization in high-strain, high-strain-rate deformation of tantalum, Mater. Sci. Eng. A. 229 (1997) 23–41.

[3] S. V. Razorenov, G. Garkushin, G.I. Kanel, O.N. Ignatova, The spall strength and Hugoniot elastic limit of tantalum with various grain size, in: AIP Conf. Proc., 2012: pp. 991–994.

[4] M.D. Furnish, L.C. Chhabildas, D.J. Steinberg, Dynamical behavior of tantalum, in: AIP Conf. Proc., AIP, 1994: pp. 1099–1102.

[5] M.D. Furnish, D.H. Lassila, L.C. Chhabildas, D.J. Steinberg, Dynamic material properties of refractory metals: tantalum and tantalum/tungsten alloys, in: AIP Conf. Proc., AIP, 1996: pp. 527–530.

[6] G.T. Gray, K.S. Vecchio, Influence of peak pressure and temperature on the structure/property response of shock- loaded Ta and Ta-10W, Metall. Mater. Trans. A. 26 (1995) 2555–2563.

[7] C.H. Lu, B.A. Remington, B.R. Maddox, B. Kad, H.S. Park, M. Kawasaki, T.G. Langdon, M.A. Meyers, Laser compression of nanocrystalline tantalum, Acta Mater. 61 (2013) 7767–7780.

[8] L.M. Hsiung, D.H. Lassila, Shock-induced deformation twinning and omega transformation in tantalum and tantalum–tungsten alloys, Acta Mater. 48 (2000) 4851–4865.

[9] L.L. Hsiung, On the Micromechanisms of Shock-Induced Martensitic Transformation in Tantalum, in: AIP Conf. Proc., AIP, 2006: pp. 228–231.

[10] J.N. Florando, B.S. El-Dasher, C. Chen, D.C. Swift, N.R. Barton, J.M. McNaney, K.T. Ramesh, K.J. Hemker, M. Kumar, Effect of strain rate and dislocation density on the twinning behavior in tantalum, AIP Adv. 6 (2016) 45120.

[11] L.L. Hsiung, Shock-induced phase transformation in tantalum, J. Phys. Condens. Matter. 22 (2010) 385702.

[12] J.N. Florando, N.R. Barton, B.S. El-Dasher, J.M. McNaney, M. Kumar, Analysis of deformation twinning in tantalum single crystals under shock loading conditions, J. Appl. Phys. 113 (2013) 83522.

[13] C.H. Lu, B.A. Remington, B.R. Maddox, B. Kad, H.S. Park, S.T. Prisbrey, M.A. Meyers, Laser compression of monocrystalline tantalum, Acta Mater. 60 (2012) 6601–6620.

[14] V. Livescu, J.F. Bingert, T.A. Mason, Deformation twinning in explosively-driven tantalum, Mater. Sci. Eng. A. 556 (2012) 155–163.

[15] M.A. Meyers, O. Vöhringer, V.A. Lubarda, The onset of twinning in metals: a constitutive description, Acta Mater. 49 (2001) 4025–4039.

[16] G.T. Gray, L.M. Hull, J.R. Faulkner, M.E. Briggs, E.K. Cerreta, F.L. Addessio, N.K. Bourne, M. Elert, M.D. Furnish, W.W. Anderson, W.G. Proud, W.T.

Butler, The effects of shock wave profile shape and shock obliquity on spallation: kinetic and stress-state effects on damage evolution, in: AIP Conf. Proc., 2009: pp. 1097–1102.

[17] C.S. Smith, Metallographic Studies of Metals after Explosive Shock, Trans. Met. Soc. A.I.M.E. 212 (1958) 574.

[18] P.S. Follansbee, G.T. Gray, Dynamic deformation of shock prestrained copper, Mater. Sci. Eng. A. 138 (1991) 23–31.

[19] N.K. Bourne, G.T. Gray, III, Computational design of recovery experiments for ductile metals, Proc. R. Soc. A Math. Phys. Eng. Sci. 461 (2005) 3297–3312.

[20] N.K. Bourne, G.T. Gray, J.C.F. Millett, On the shock response of cubic metals, J. Appl. Phys. 106 (2009) 91301.

[21] N.K. Bourne, Materials' Physics in Extremes: Akrology, Metall. Mater. Trans. A. 42 (2011) 2975–2984.

[22] O.T. Strand, L. V Berzins, D.R. Goosman, W.W. Kuhlow, P.D. Sargis, T.L. Whitworth, Velocimetry using heterodyne techniques, in: D.L. Paisley, S. Kleinfelder, D.R. Snyder, B.J. Thompson (Eds.), SPIE Proc., 2005: p. 593.

[23] B. Pang, I.P. Jones, Y.-L. Chiu, J.C.F. Millett, G. Whiteman, Electron channelling contrast imaging of dislocations in a conventional SEM, Philos. Mag. 97 (2017) 346–359.

[24] M.H. Loretto, R.E. Smallman, Defect Analysis in Electron Microscopy, Springer US, 1975.

[25] M.A. Meyers, Dynamic Behavior of Materials, John Wiley & Sons, Inc., Hoboken, NJ, USA, 1994.

[26] R. Kinslow, ed., High Velocity Impact Phenomena, Academic Press, Inc. (London) LTD., 1970.

[27] B. Pang, I. Jones, Y. Chiu, J. Millett, G. Whiteman, N. Bourne, Orientation dependence of shock induced dislocations in tantalum single crystals, J. Phys. Conf. Ser. 522 (2014) 12029.

[28] I. MacDonald, Development of a 3D Lagrangian/ALE hydrocode, Proc. Int. Work. New Model. Numer. Codes Shock Wave Process. Condens. Media. (1997) 810–814.

[29] C.A. Bronkhorst, B.L. Hansen, E.K. Cerreta, J.F. Bingert, Modeling the microstructural evolution of metallic polycrystalline materials under localization conditions, J. Mech. Phys. Solids. 55 (2007) 2351–2383.

[30] S.N. Kuchnicki, R.A. Radovitzky, A.M. Cuitiño, An explicit formulation for multiscale modeling of bcc metals, Int. J. Plast. 24 (2008) 2173–2191.

[31] A. Mandal, Y.M. Gupta, Elastic-plastic deformation of molybdenum single

crystals shocked along [100], J. Appl. Phys. 121 (2017) 45903.

[32] D. Grady, Shock Equation of State Properties of Concrete, in: C.A. Brebbia, N. Jones, A.J. Watson (Eds.), Struct. under Shock Impact IV, Southampton, 1996: pp. 405–414.

[33] T. Antoun, L. Seaman, D.R. Curran, G.I. Kanel, S. V. Razorenov, A. V. Utkin, Spall Fracture, Springer New York, 2006.

[34] F.A. McClintock, Ductility: Papers Presented at a Seminar of the American Society for Metals, in: American Society for Metals, 1968: p. 255.

[35] P.F. Thomason, A Theory for Ductile Fracture by Internal Necking of Cavities, J. Inst. Met. 98 (1968) 360.

[36] L.M. Brown, J.D. Embury, The Initiation and Growth of Voids at Second Phase Particles, in: Proc. 3rd Int. Conf. Strength Met. Alloy., 1973: pp. 571–582.

[37] L. Davison, R.. Graham, Shock compression of solids, Phys. Rep. 55 (1979) 255–379.

[38] H. Wang, D.S. Xu, R. Yang, Atomic modelling of crack initiation on twin boundaries in α-titanium under external tensile loading along various orientations, Philos. Mag. Lett. 94 (2014) 779–785.

[39] E.N. Hahn, T.C. Germann, R. Ravelo, J.E. Hammerberg, M.A. Meyers, On the ultimate tensile strength of tantalum, Acta Mater. 126 (2017) 313–328.

[40] E.N. Hahn, T.C. Germann, R.J. Ravelo, J.E. Hammerberg, M.A. Meyers, Non-equilibrium molecular dynamics simulations of spall in single crystal tantalum, in: AIP Conf. Proc., 2017: p. 70006.

[41] A.S. Appleton, J.S. Waddington, The importance of shock wave profile in explosive loading experiments, Acta Metall. 12 (1964) 956–957.

[42] L.E. Murr, Effects of Peak Pressure, Pulse Duration, and Repeated Loading on the Residual Structure and Properties of Shock Deformed Metals and Alloys, in: Shock Waves High-Strain-Rate Phenom. Met., Springer US, Boston, MA, 1981: pp. 753–777.

[43] J.B. Cohen, J. Weertman, A dislocation model for twinning in f.c.c. metals, Acta Metall. 11 (1963) 996–998.

[44] J.R. Asay, High-Pressure Shock Compression of Solids, Springer New York, 2012.

[45] P.P. Gillis, K.G. Hoge, R.J. Wasley, Elastic Precursor Decay in Tantalum, J. Appl. Phys. 42 (1971) 2145–2146.

[46] J.W. Taylor, Dislocation Dynamics and Dynamic Yielding, J. Appl. Phys. 36 (1965) 3146–3150.

[47] R.W. Rohde, Metallurgical Effects at High Strain Rates, Springer US, Boston,

MA, 1973.

[48] M. Knezevic, I.J. Beyerlein, M.L. Lovato, C.N. Tomé, A.W. Richards, R.J. McCabe, A strain-rate and temperature dependent constitutive model for BCC metals incorporating non-Schmid effects: Application to tantalum-tungsten alloys, Int. J. Plast. 62 (2014) 72–92.

[49] R. Ravelo, T.C. Germann, O. Guerrero, Q. An, B.L. Holian, Shock-induced plasticity in tantalum single crystals: Interatomic potentials and large-scale molecular-dynamics simulations, Phys. Rev. B. 88 (2013) 134101.

[50] D. Hull, D.J. Bacon, Introduction to Dislocations, Elsevier Science, 2001.

Table 1 Summary of the twin distribution in the shocked single crystals (see also Figure 5)

Sample	Shock interface (Region 1)		Sample front centre (Region 2)		Sample bottom right side (Region 3)	
	Twin planes	Comment	Twin planes	Comment	Twin planes	Comment
[001]	$(2\bar{1}1)$, (211), (121), $(\bar{1}21)$, $(2\bar{1}\bar{1})$, $(21\bar{1})$, $(12\bar{1})$, $(\bar{1}2\bar{1})$	Twin-free at centre	$(2\bar{1}1)$, (211), (121), $(\bar{1}21)$, $(2\bar{1}\bar{1})$, $(21\bar{1})$, $(12\bar{1})$, $(\bar{1}2\bar{1})$	0-0.1 mm under front surface: twin free; 0.1-4 mm from front surface: area fraction decreases with distance from front surface	$(2\bar{1}\bar{1})$	Only one type of twin
[011]	(211), $(\bar{2}11)$	Homogeneously distributed over front surface, same as region 2	(211), $(\bar{2}11)$	No twin free region; area fraction decreases with distance from front surface.	$(\bar{2}11)$	Only one type of twin
[111]	(112), (121), (211)	Homogeneously distributed over front surface, same as region 2	(112), (121), (211)	No twin free region; area fraction decreases with distance from front surface.	(121)	Only one type of twin

Table 2 Summary of dislocation Burgers vectors observed

Specimen	Region A	Region B	Directions	
	Dominant Burgers vectors			
[001]	$\frac{1}{2}[\bar{1}11], \frac{1}{2}[1\bar{1}1]$	$\frac{1}{2}[\bar{1}11], \frac{1}{2}[1\bar{1}1]$	SWD	$[00\bar{1}]$
			RWD	$[\bar{1}10]$
[011]	$\frac{1}{2}[111], \frac{1}{2}[\bar{1}11]$	$\frac{1}{2}[111], \frac{1}{2}[\bar{1}11], \frac{1}{2}[1\bar{1}1], \frac{1}{2}[11\bar{1}]$	SWD	$[0\bar{1}\bar{1}]$
			RWD	[100]
[111]	$\frac{1}{2}[111], \frac{1}{2}[\bar{1}11], \frac{1}{2}[1\bar{1}1], \frac{1}{2}[11\bar{1}]$	$\frac{1}{2}[111], \frac{1}{2}[\bar{1}11], \frac{1}{2}[1\bar{1}1], \frac{1}{2}[11\bar{1}]$	SWD	$[\bar{1}\bar{1}\bar{1}]$
			RWD	$[\bar{1}2\bar{1}]$

Table 3 Shear stresses σ_{xy} for twinning systems in the tantalum single crystals under shock loading with unit compression stress. These stresses are effectively the Schmid factors for the twinning systems. A positive σ_{xy} means the stress favours twinning and negative σ_{xy} means it is in the anti-twin direction.

001			011			111		
Twinning plane	Shear direction	σ_{xy}	Twinning plane	Shear direction	σ_{xy}	Twinning plane	Shear direction	σ_{xy}
(211)	$[\bar{1}11]$	0.236	(211)	$[\bar{1}11]$	0.471	(211)	$[\bar{1}11]$	0.314
$(21\bar{1})$	$[\bar{1}1\bar{1}]$	0.236	$(21\bar{1})$	$[\bar{1}1\bar{1}]$	0	$(21\bar{1})$	$[\bar{1}1\bar{1}]$	-0.157
$(2\bar{1}1)$	$[\bar{1}\bar{1}1]$	0.236	$(2\bar{1}1)$	$[\bar{1}\bar{1}1]$	0	$(2\bar{1}1)$	$[\bar{1}\bar{1}1]$	-0.157
$(\bar{1}2\bar{1})$	[111]	0.236	$(\bar{1}2\bar{1})$	[111]	-0.236	$(\bar{1}2\bar{1})$	[111]	0
$(12\bar{1})$	$[1\bar{1}\bar{1}]$	0.236	$(12\bar{1})$	$[1\bar{1}\bar{1}]$	-0.236	$(12\bar{1})$	$[1\bar{1}\bar{1}]$	-0.157
$(1\bar{1}\bar{2})$	$[1\bar{1}1]$	-0.471	$(1\bar{1}\bar{2})$	$[1\bar{1}1]$	0	$(1\bar{1}\bar{2})$	$[1\bar{1}1]$	-0.157
$(\bar{1}21)$	$[11\bar{1}]$	0.236	$(\bar{1}21)$	$[11\bar{1}]$	0	$(\bar{1}21)$	$[11\bar{1}]$	-0.157
$(11\bar{2})$	[111]	-0.471	$(11\bar{2})$	[111]	-0.236	$(11\bar{2})$	[111]	0
$(1\bar{1}2)$	$[1\bar{1}\bar{1}]$	-0.471	$(1\bar{1}2)$	$[1\bar{1}\bar{1}]$	-0.236	$(1\bar{1}2)$	$[1\bar{1}\bar{1}]$	-0.157
(112)	$[11\bar{1}]$	-0.471	(112)	$[11\bar{1}]$	0	(112)	$[11\bar{1}]$	0.314
(121)	$[1\bar{1}1]$	0.236	(121)	$[1\bar{1}1]$	0	(121)	$[1\bar{1}1]$	0.314
$(2\bar{1}\bar{1})$	[111]	0.236	$(2\bar{1}\bar{1})$	[111]	0.471	$(2\bar{1}\bar{1})$	[111]	0

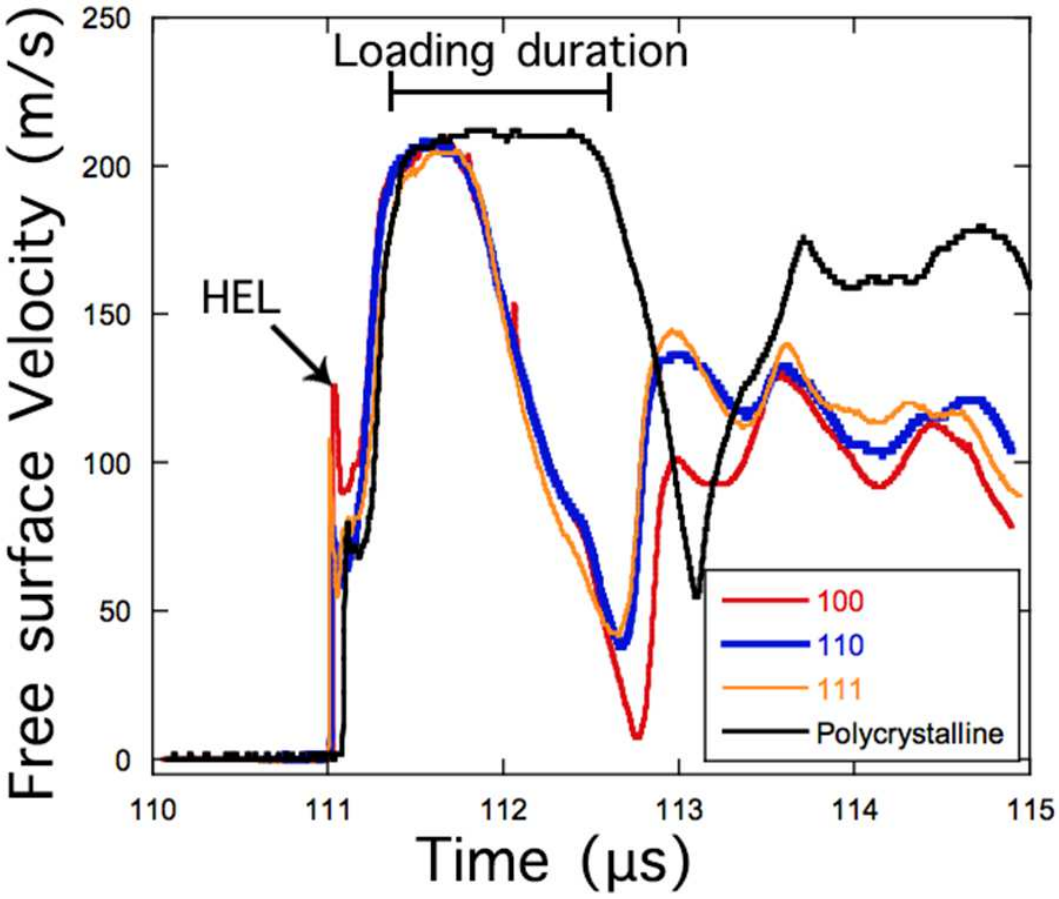

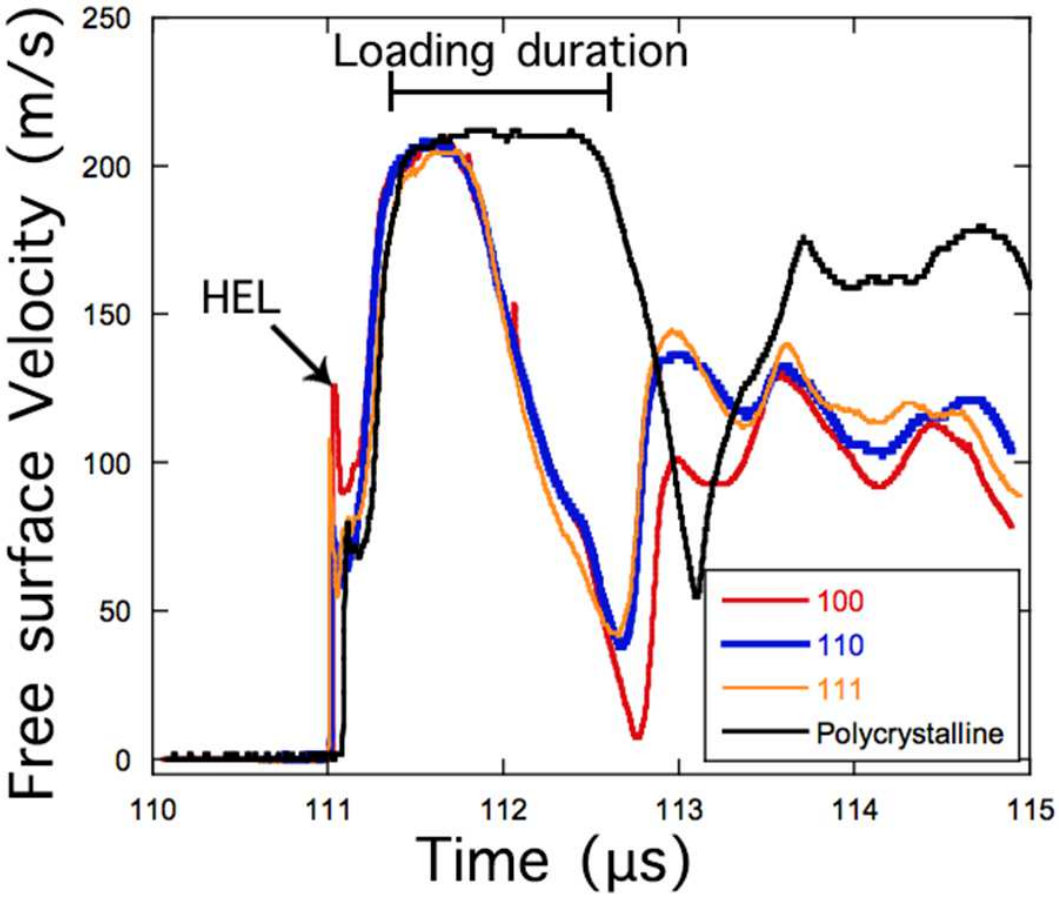

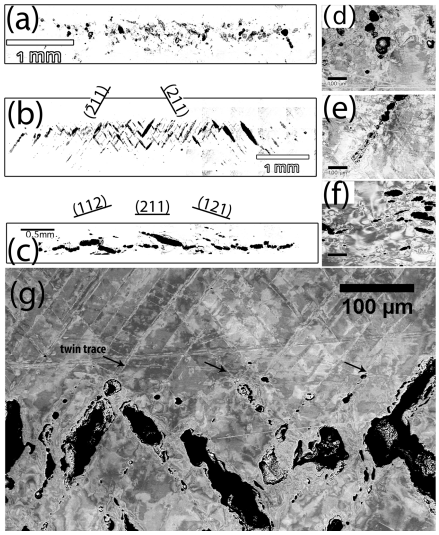

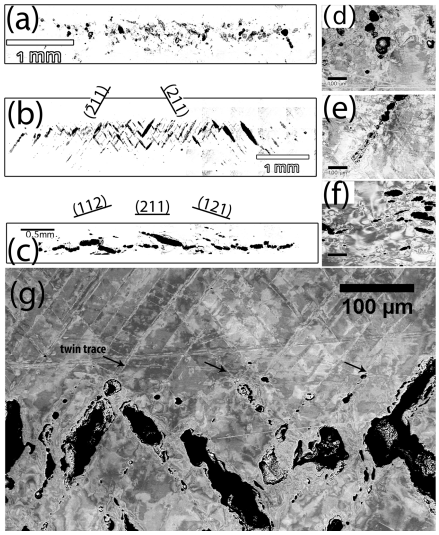

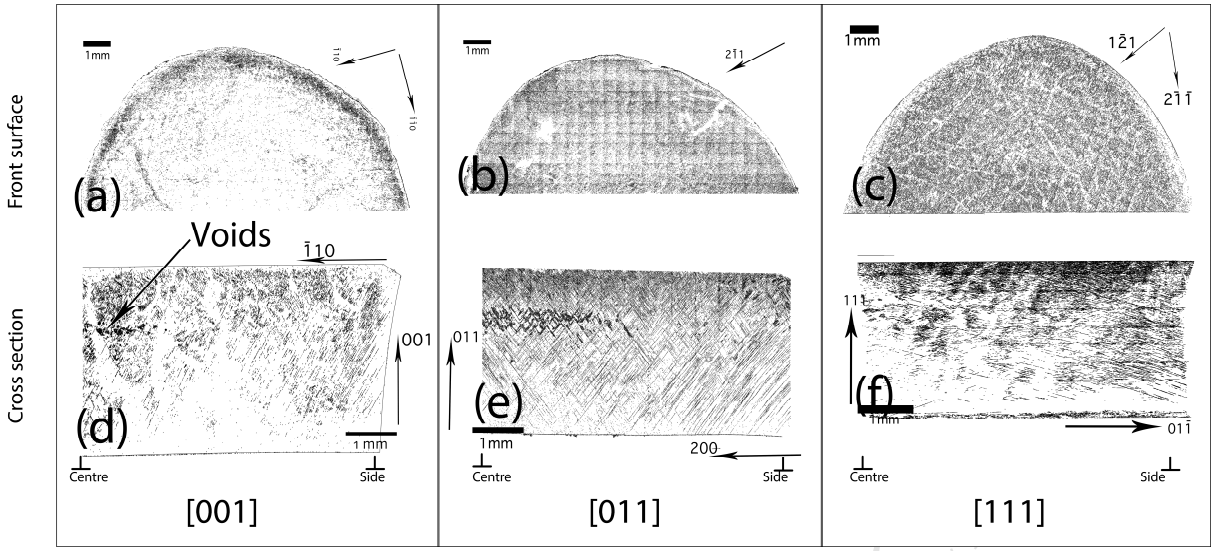

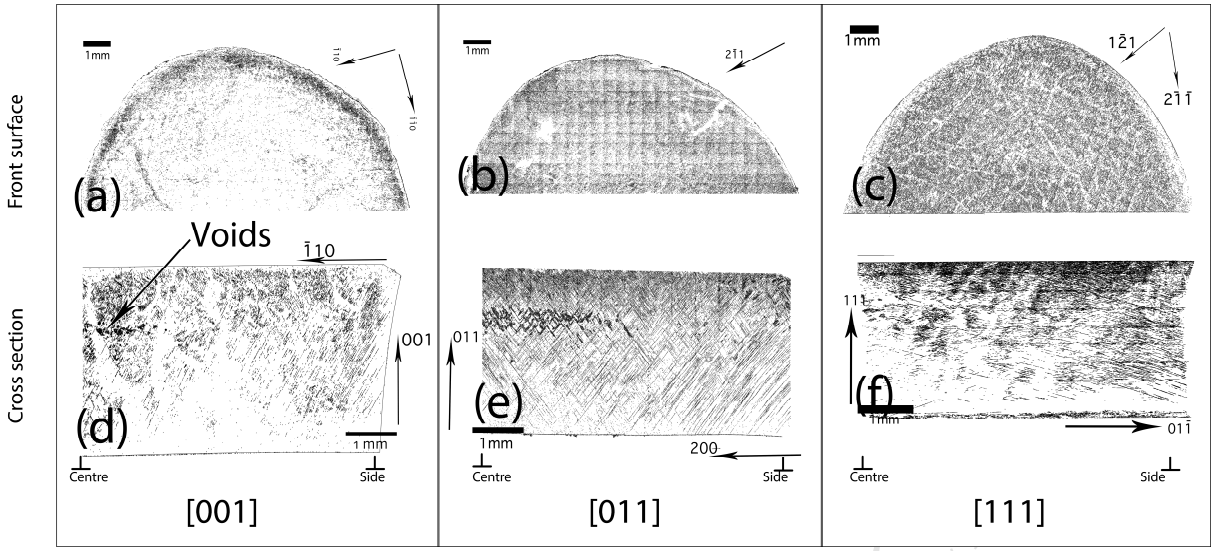

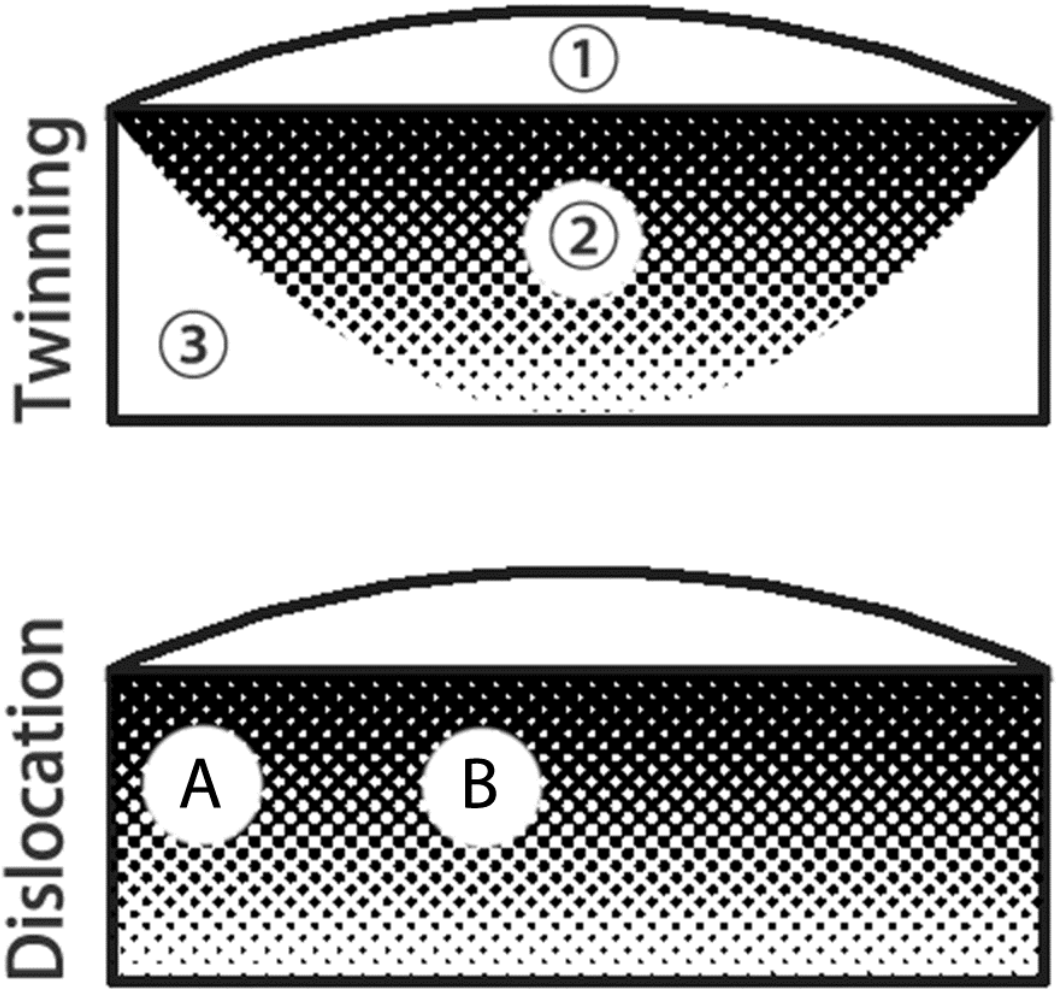

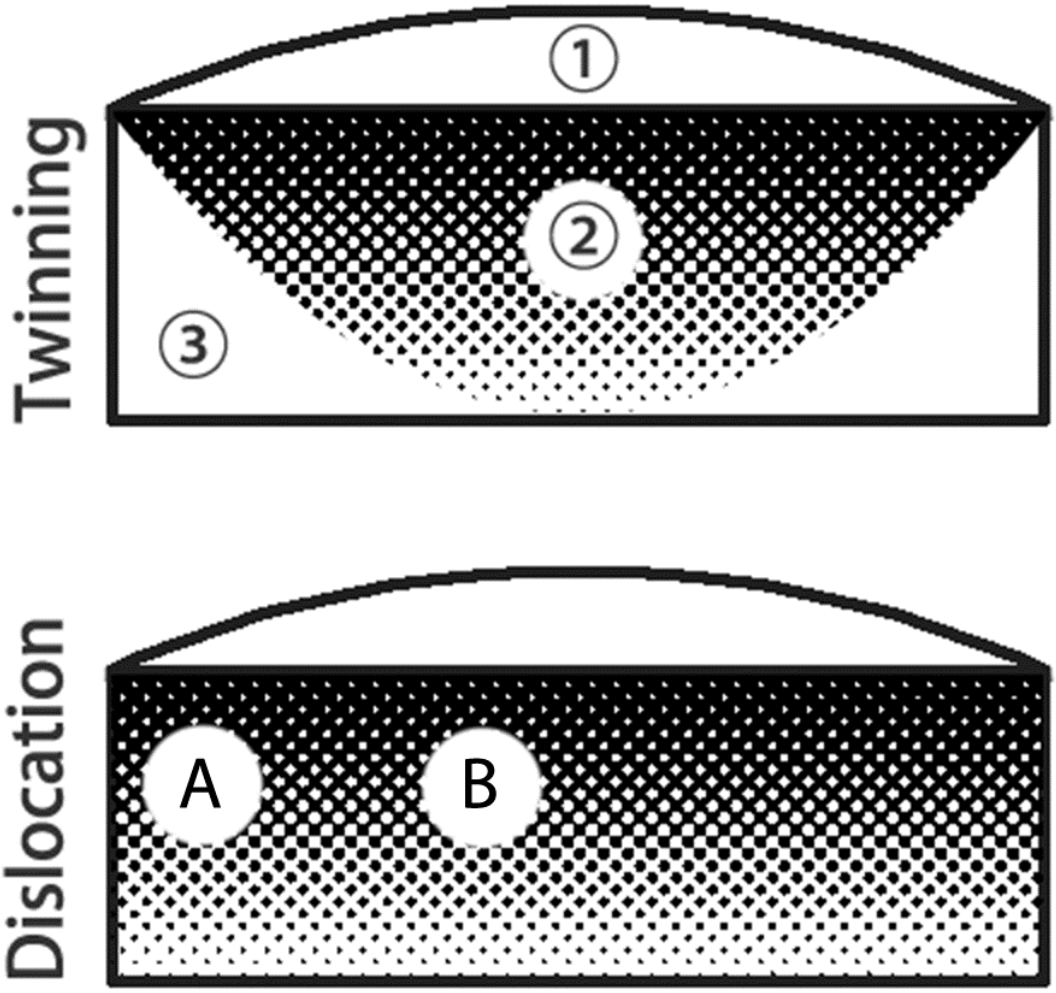

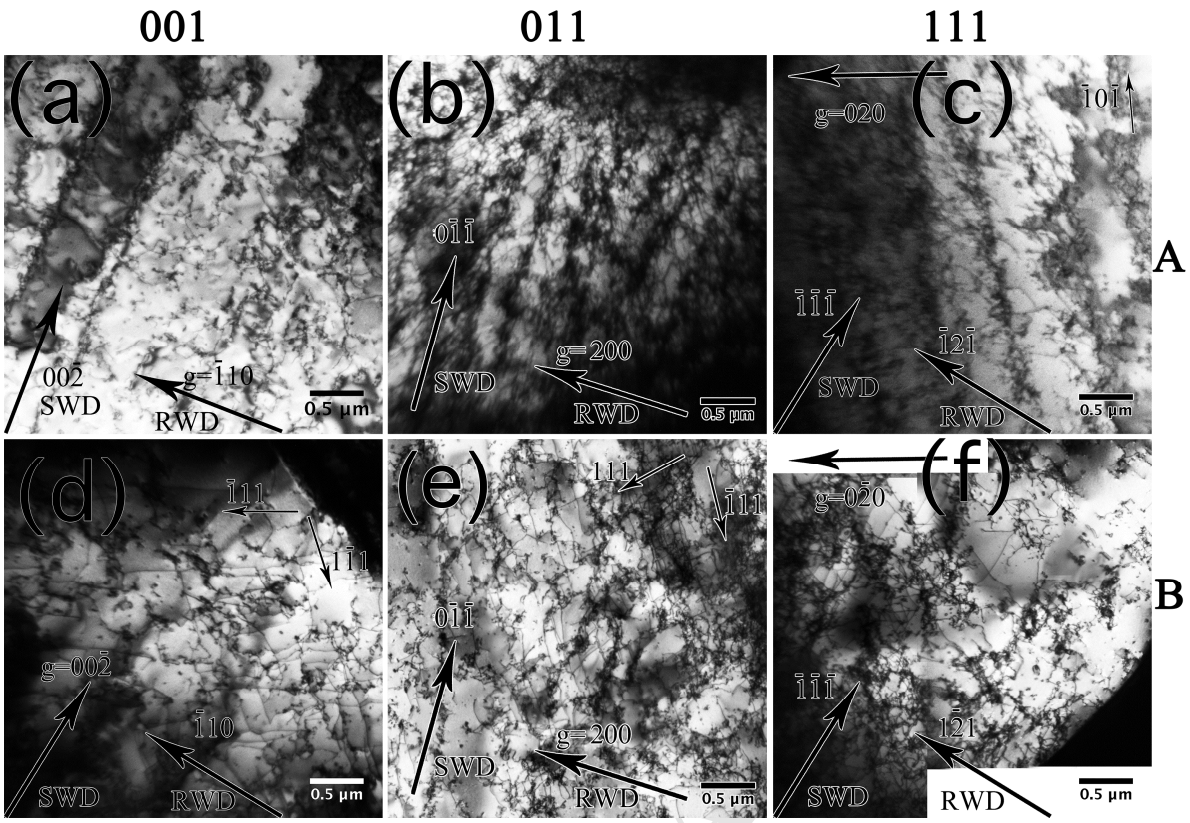

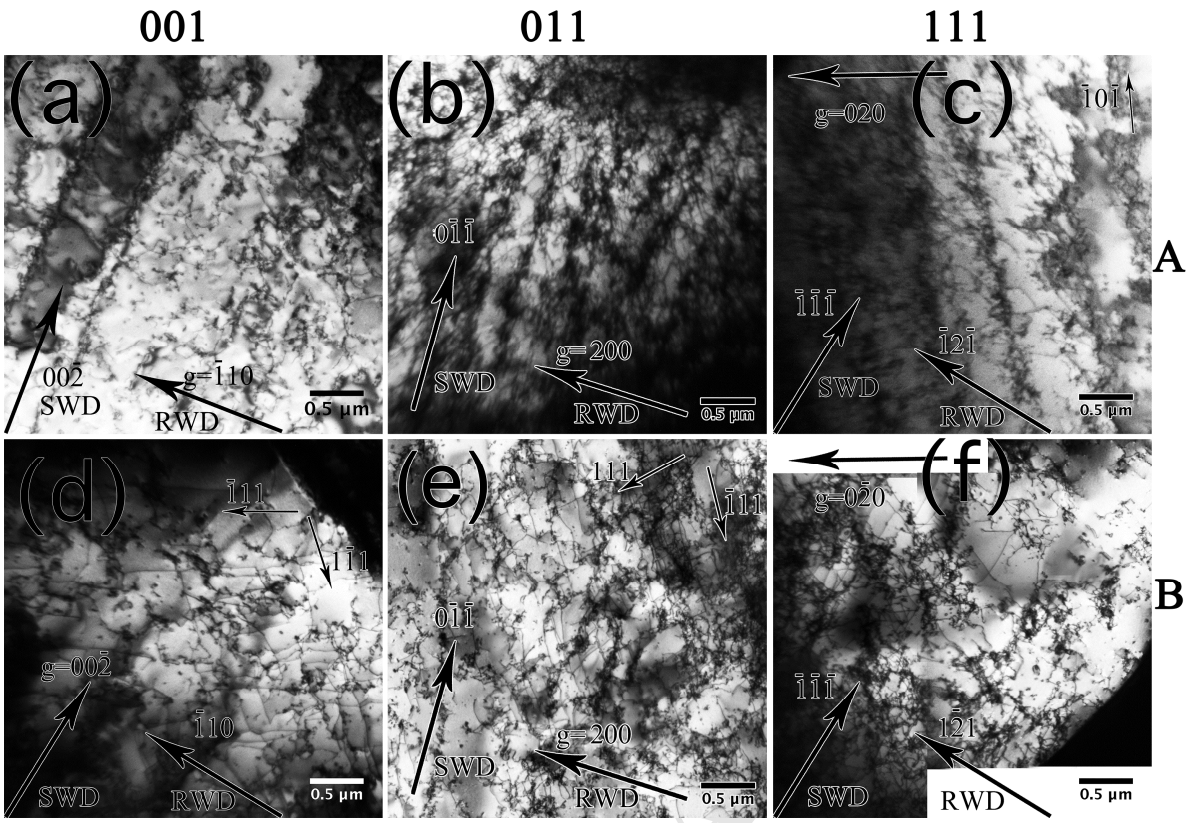

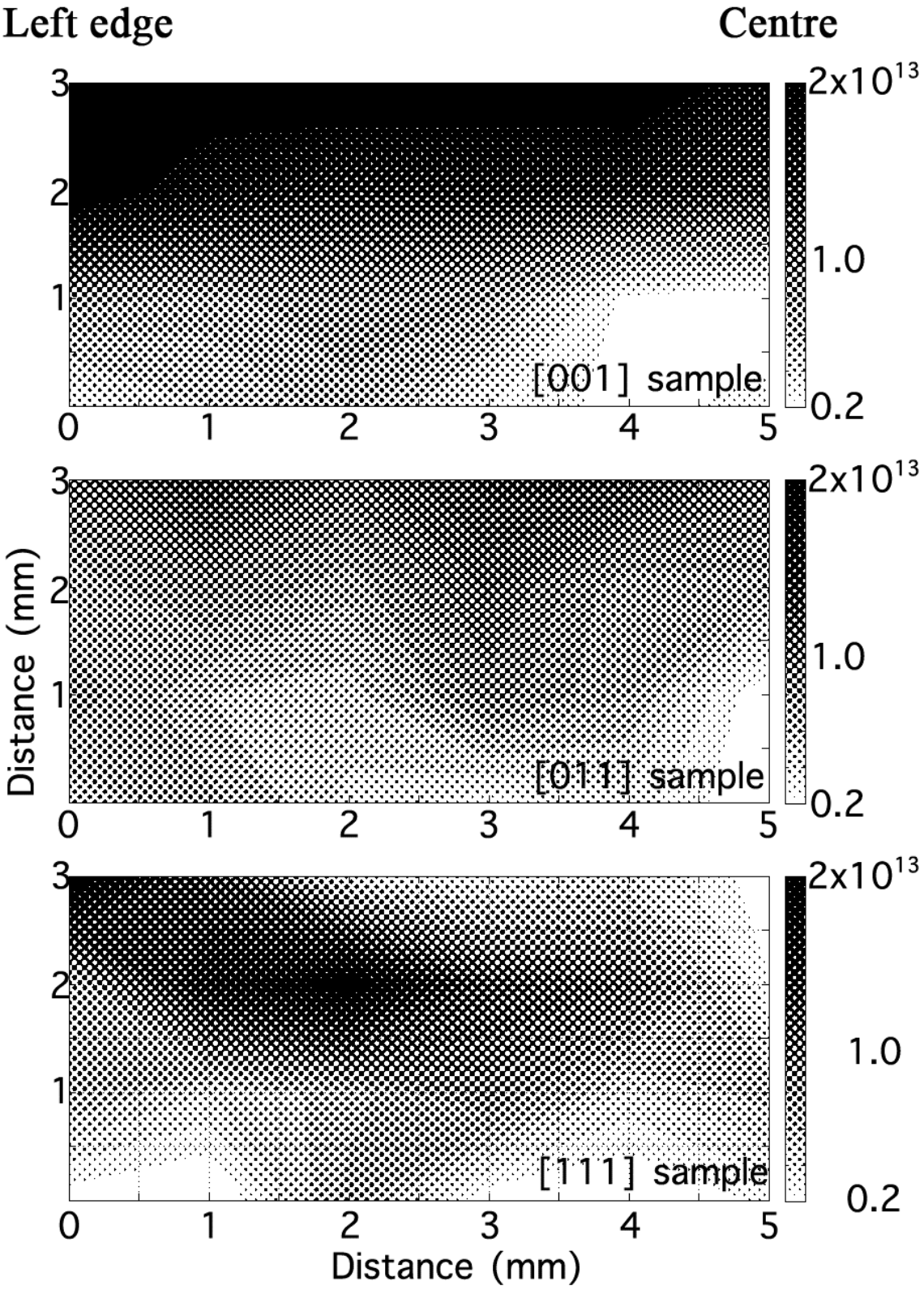
Left edge
Centre
[001] sample
[011] sample
[111] sample
Distance (mm)
Distance (mm)
2x10^13
1.0
0.2
0
1
2
3
4
5

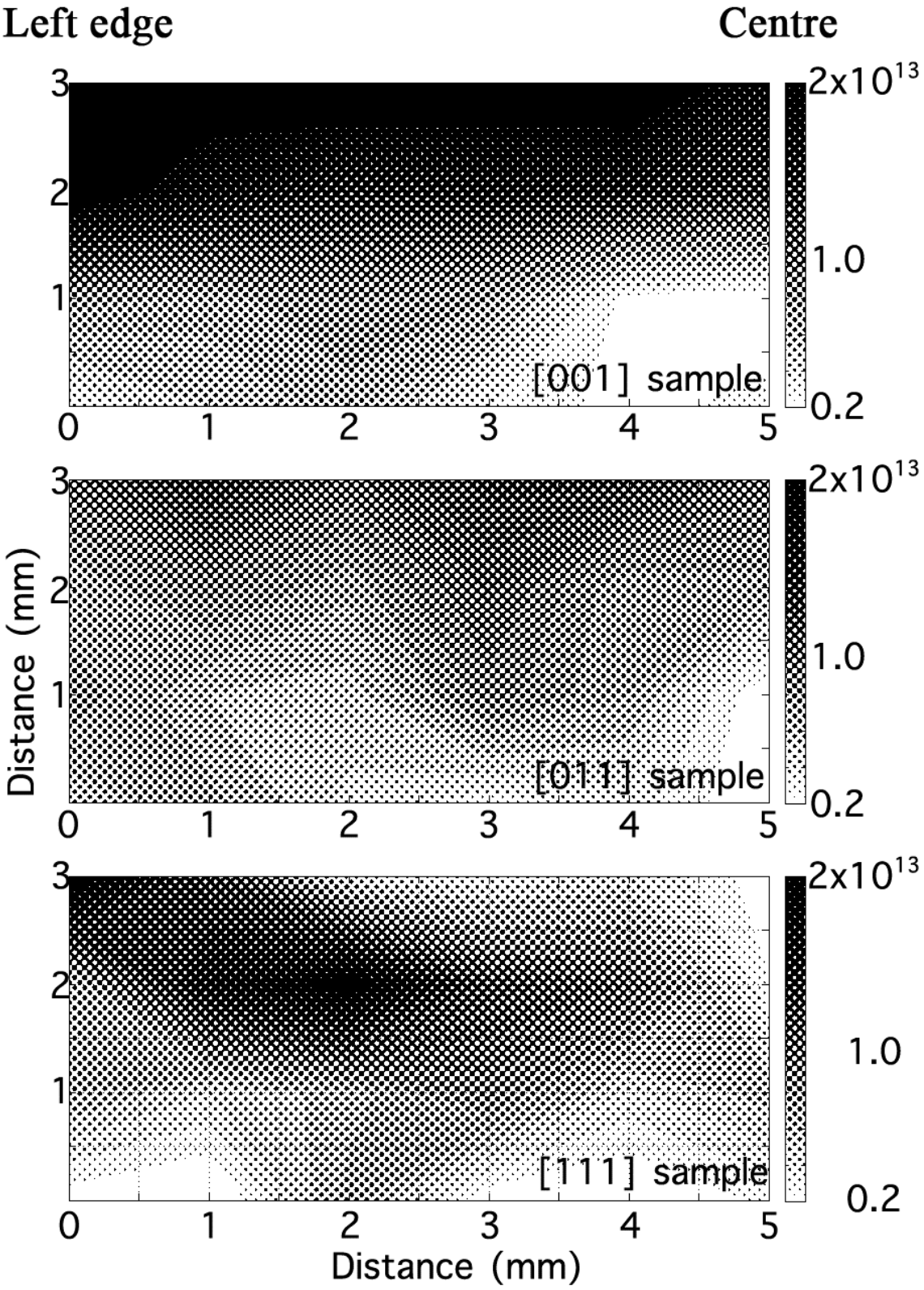
Left edge
Centre
[001] sample
[011] sample
[111] sample
Distance (mm)
Distance (mm)
2x10^13
1.0
0.2
0
1
2
3
4
5

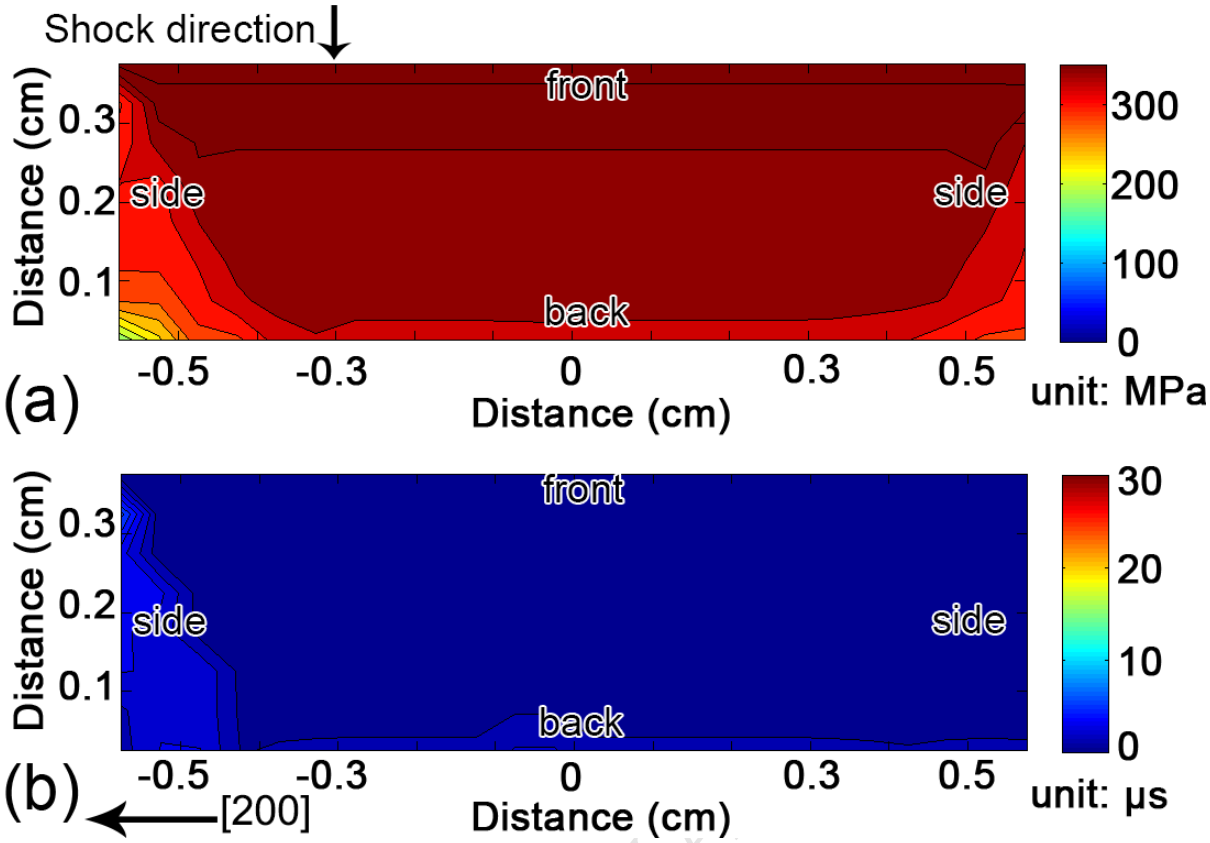

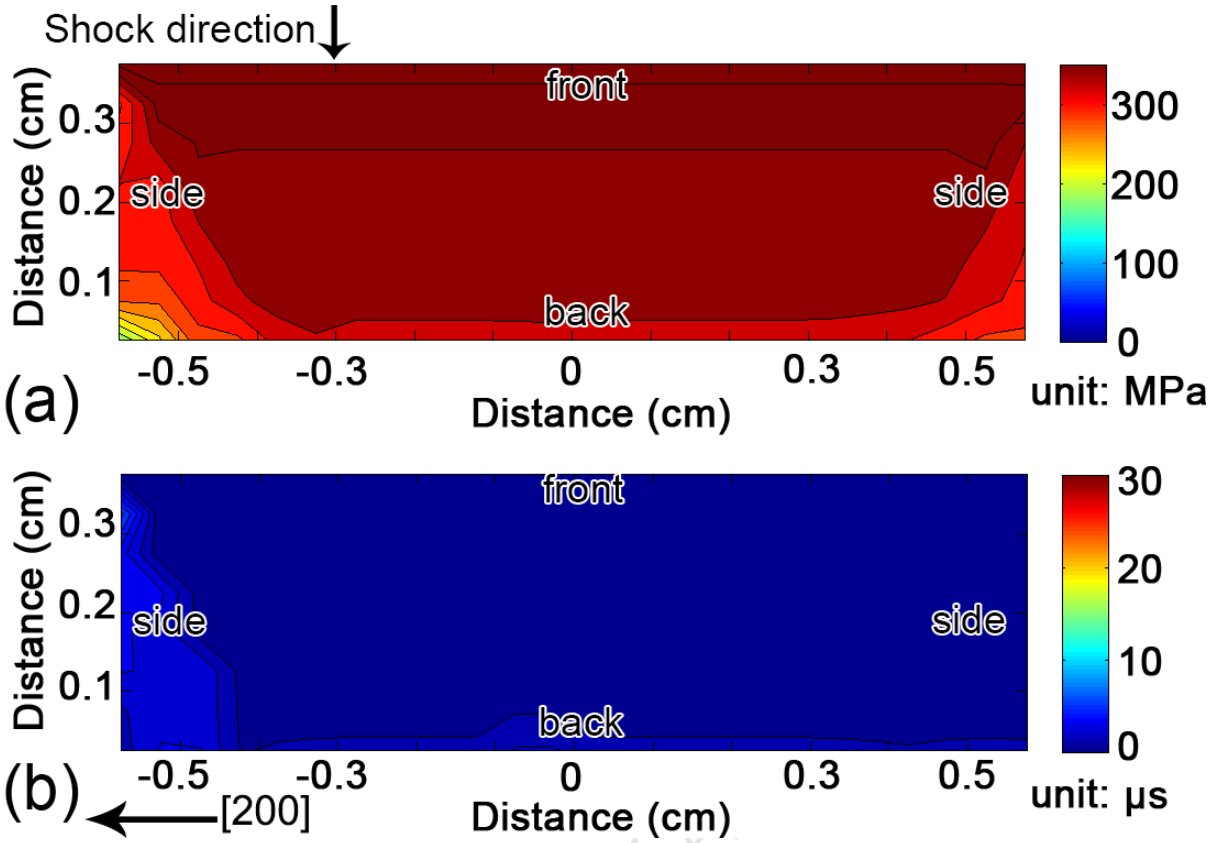

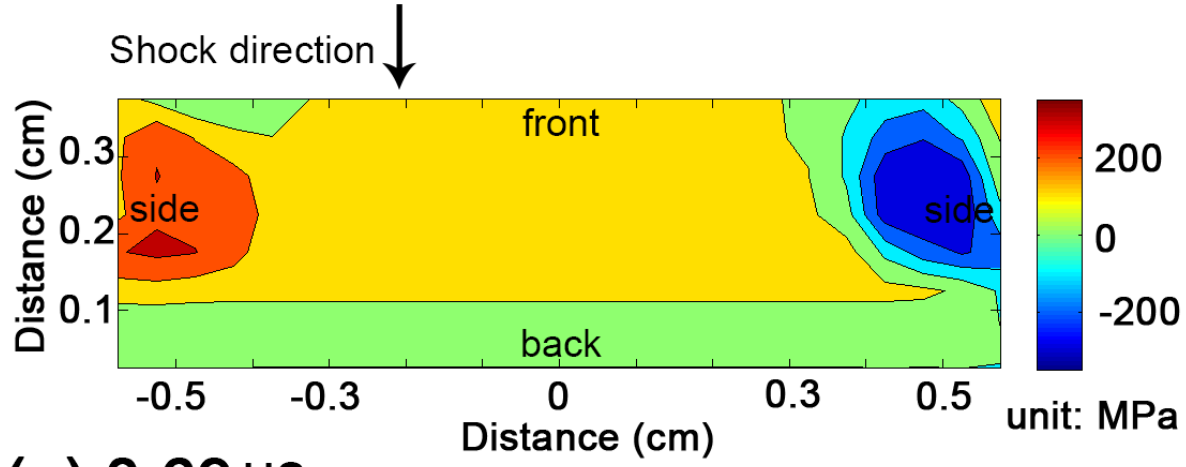

(a) 0.69 μs

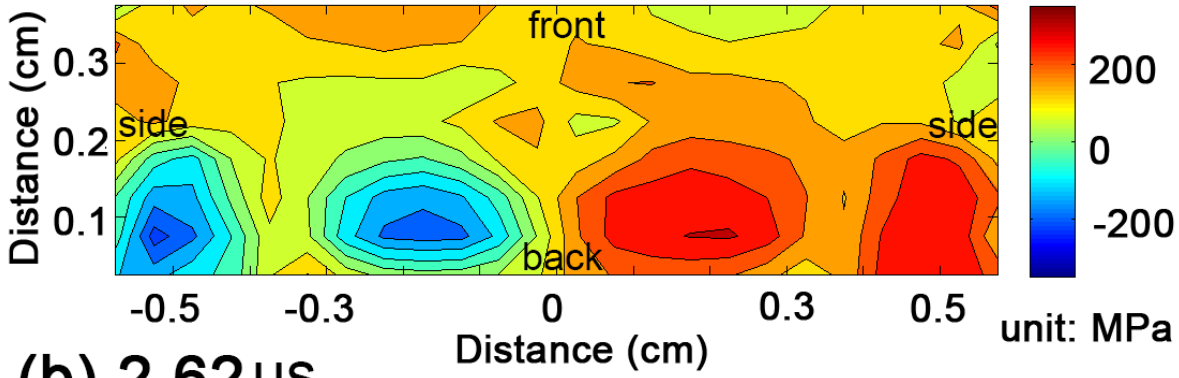

(b) 2.62 μs

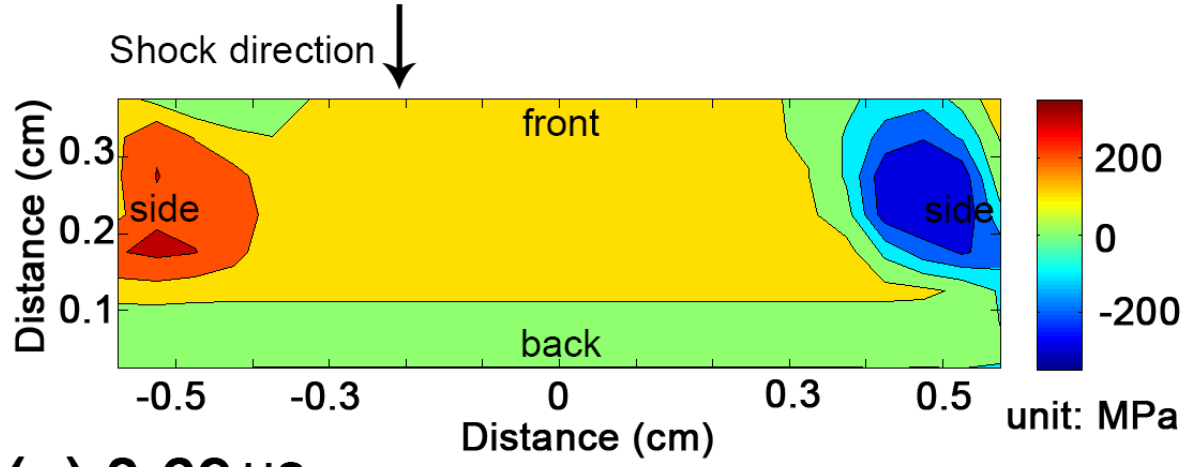

(a) 0.69 μs

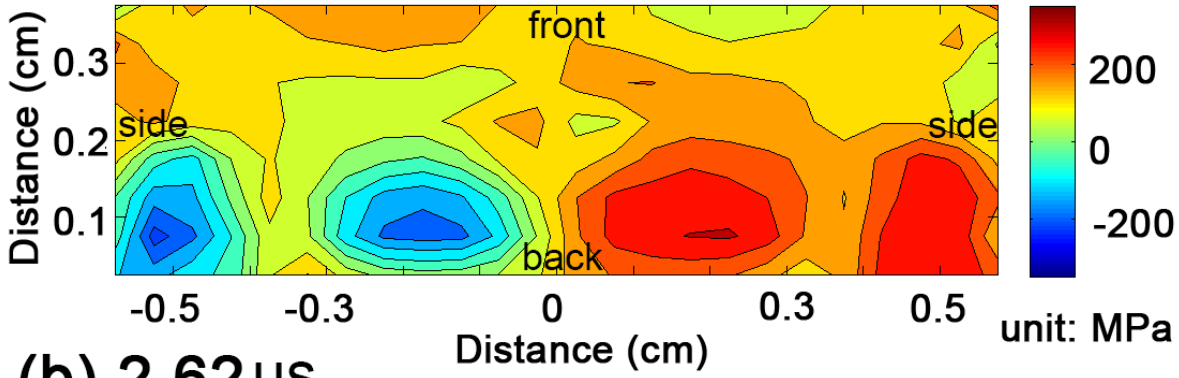

(b) 2.62 μs

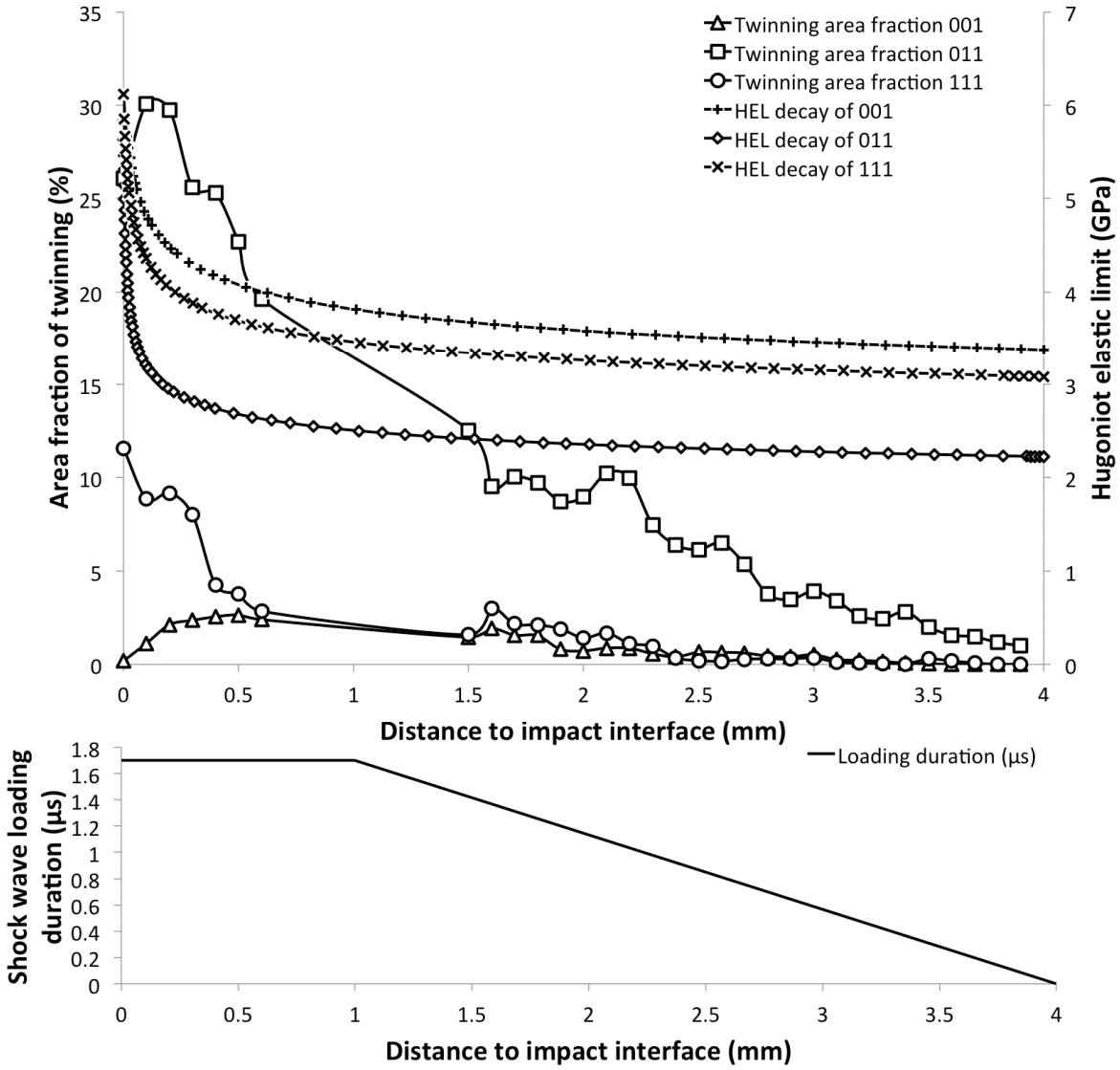
Twinning area fraction 001
Twinning area fraction 011
Twinning area fraction 111
HEL decay of 001
HEL decay of 011
HEL decay of 111
Area fraction of twinning (%)
Hugoniot elastic limit (GPa)
Distance to impact interface (mm)
Loading duration (μs)
Shock wave loading duration (μs)
Distance to impact interface (mm)

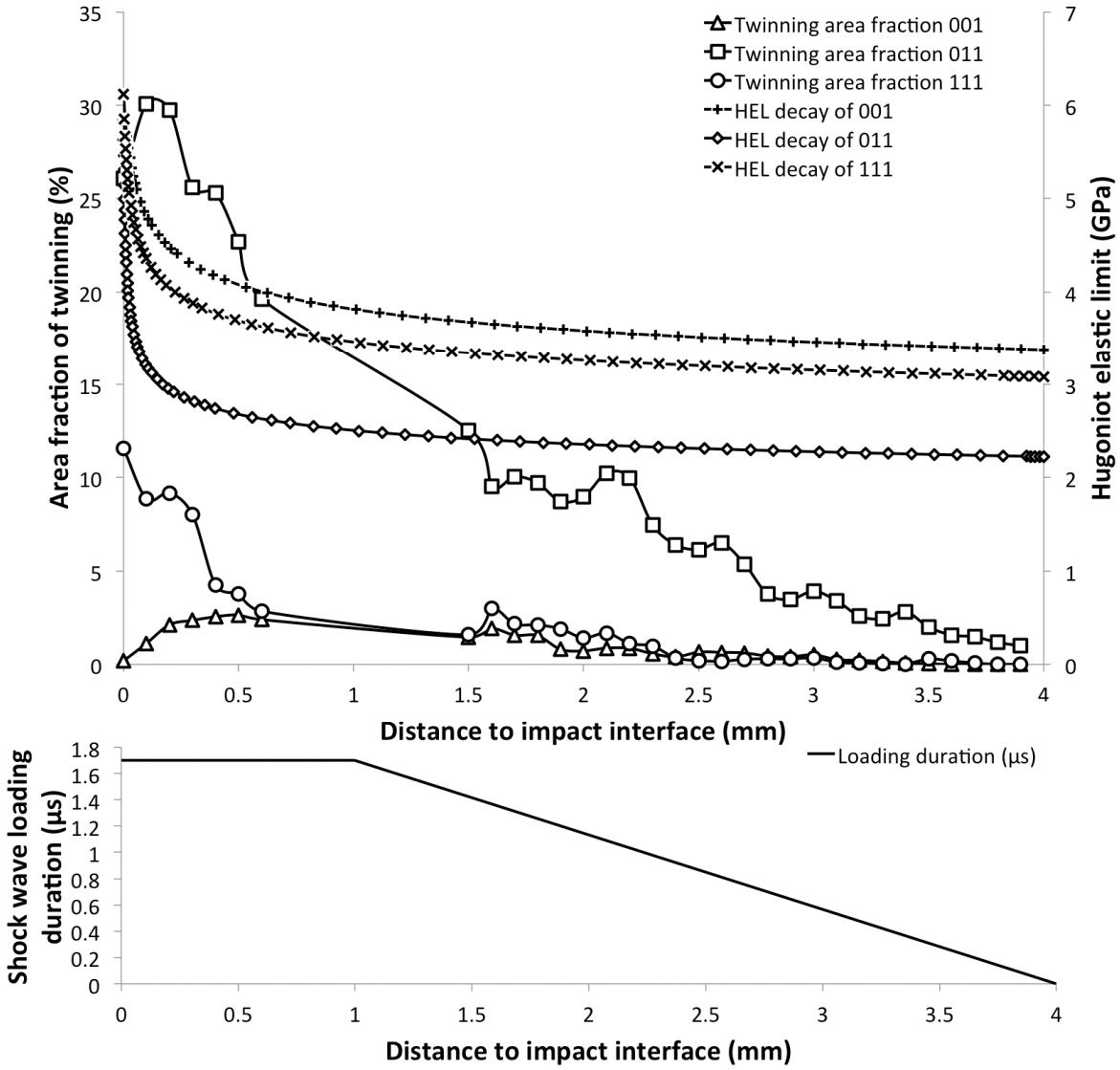
Twinning area fraction 001
Twinning area fraction 011
Twinning area fraction 111
HEL decay of 001
HEL decay of 011
HEL decay of 111
Area fraction of twinning (%)
Hugoniot elastic limit (GPa)
Distance to impact interface (mm)
Loading duration (μs)
Shock wave loading duration (μs)
Distance to impact interface (mm)